Proximity Effect in Transient Analysis of Radio Base Stations

Hongcai Chen, Yaping Du[1]
Dept. of Building Services Engineering, The Hong Kong Polytechnic University
Hung Hom, Kowloon, Hong Kong
[1]ya-ping.du@polyu.edu.hk

SUMMARY

This paper presents an equivalent circuit model for calculating fast transient current distribution in radio base station system. The new model takes account of both skin and proximity effects in the simulation and achieves a fast computation by using an efficient discretization scheme. The obtained circuit is synthesized using a time domain solver, PSpice. The proposed method is validated experimentally, and is applied to evaluate the lightning current in a practical radio base station. A practical system with a 20 m tower and 7 cables is analysed. Various surge protective devices (SPD) are installed among cables in the simulation. Comparison among different configurations reveals that proximity effect will lead to uneven current distribution in cables. Outer-located cables will carry more currents than others which should be paid more attention.

KEYWORDS: skin effect; proximity effect; lightning transient; power cable; PEEC; EMC

I. INTRODUCTION

Electric cables are the essential components in electric power systems. These cables may be exposed to lightning or other unpredictable transients, and carry substantial transient currents. This certainly increases the risk of transient-generated damage in connected equipment. To provide effective protection for vulnerable equipment, it is necessary to carry out transient current analysis in the systems, which requires appropriate cable modeling. It is known that power cables exhibit significant skin and proximity effects under the lightning transient current. In addition, the metallic structure, such as a tower or rack may conduct substantial transient currents as well. These factors need to be considered in cable modelling.

For simplicity, the proximity effect was sometimes neglected in transient analysis [1, 2]. Supporting wire structures are usually not included [3, 4], or simply represented with a distributed impedance [5]. In fact, the proximity effect and the adjacent structures could have a great impact on the current distribution, especially among closely spaced conductors. Cable modelling without considering these factors could lead to significant errors in analyzing transient current carried by the cables. For example, in a radio base station supplied at 48VDC small errors in modeling cables can cause misleading results when the system carried a lightning discharge current.

Numerical methods have been developed for modeling cables, such as transmission line method (TL) [3, 6], finite element method (FEM) [7, 8], finite difference time domain (FDTD) [1, 9], partial element equivalent circuit method [10, 11] (PEEC), etc. Among these methods, the PEEC method, which transforms the EM problems into equivalent circuits, is a great alternative for cable simulation. It is convenient to integrate obtained PEEC elements with various surge protective devices (SPDs) in the simulation. Therefore, we propose a PEEC-based system modeling approach to capture both skin and proximity effects in a complex wire system. The skin effect model [12-14] is well developed using analytical expressions and is applied for isolated cables. While, a discretization PEEC formulation is proposed in order to consider the proximity effect among closely-spaced cables. A novel non-uniform meshing scheme ensures the fast calculation. The obtained frequency-dependent parameters are transformed into equivalent circuits using rational approximation. Both skin effect and proximity effect are then taken into consideration in the system model. The built system network is solved by PSpice (time domain solver) together with TAES (wire modeling tool) [2] where SPDs are easily incorporated.

The rest of the paper is organized as follows. Section II describes the theory of the proposed method. In Section III, experimental validation of the proposed model is presented. Comprehensive discussion on the influence of proximity effect is shown in Section IV. In Section V, transient currents in a practical radio base station system are evaluated.

II. EQUIVALENT CIRCUIT MODEL FOR CABLES

2.1 Basic PEEC formulation

The PEEC method [15] has been developed for modeling electromagnetic coupling among thin conductors. This method was derived from the integral form of Maxwell's equations. It is known that electric field at point r on a thin conductor can be expressed with magnetic vector potential A and electric scalar potential ϕ, as follows:

$$0 = \frac{J(r)}{\sigma} + j\omega A(r) + \nabla\phi(r) \tag{1}$$

where J is the current density at point r, σ is the electric conductivity of the conductor, and ω is the angular frequency of the current. Both vector and scalar potentials A and ϕ are expressed by

$$\begin{aligned} A(r) &= \frac{\mu}{4\pi}\int_{v'}\frac{J(r)}{|r-r'|}dv' \\ \phi(r) &= \frac{1}{4\pi\varepsilon}\int_{v'}\frac{\rho(r)}{|r-r'|}dv' \end{aligned} \tag{2}$$

in which v' is the volume of the conductor, r' is the position vector of the volume element dv', and ρ is the volume charge density. Applying the Green's functions of free space, we obtain the partial elements as listed in the table below:

TABLE I. EXPRESSIONS OF PEEC ELEMENTS

Partial Element Type	Partial Element Expression
Resistance	$R_i = \frac{l_i}{\sigma_i a_i}$
Partial inductance	$L_{ij} = \frac{\mu}{4\pi}\frac{1}{a_i a_j}\int_{V_i}\int_{V_j}\frac{1}{R}dV_i dV_j$
Coefficients of potential	$P_{ij} = \frac{1}{4\pi\varepsilon}\frac{1}{S_i S_j}\int_{S_i}\int_{S_j}\frac{1}{R}dS_i dS_j$

For lightning transient analysis, the capacitive effect among conductors is negligible due to its low frequency spectrum. Only the resistance components and inductively-coupled components retain in the circuit. Meanwhile, as the wavelength at the primary frequency of lightning currents is significantly longer than the conductor, retardation effect is negligible [16-18]. It is known that a circuit is considered electrically small when the largest dimension is smaller than one-tenth of a wavelength [19]. Thus, the quasi-static assumption is made in the calculation. A typical equivalent PEEC circuit is constructed as shown in Figure 1. In the circuit EM couplings are achieved using controlled sources.

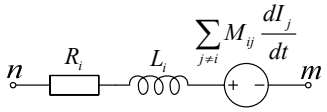

Figure 1. PEEC equivalent circuit of one segment

2.2 Discretization PEEC Model

The calculation becomes more complicated when multiple conductors exist due to the proximity effect, especially for closely spaced conductors. The currents crowd to the adjacent faces of the conductors. As no closed form equation is available, a discretization scheme is then proposed to take account of this effect. Conductors are divided into small segments over their cross sections where the current in each segment is assumed to be evenly distributed.

To avoid an extremely large number of cells, a non-uniform discretization scheme [4] is adopted, as seen in Figure 2. In the cross section of the conductor, the current density J decreases exponentially from its surface to the depth x following:

$$J = J_s \exp\left(-\frac{x}{\delta}\right) \tag{3}$$

where δ is the skin depth, and J_s is the surface current density. Therefore, we segment a conductor in the radial direction following the rule that the current decrease 10 % at each layer. The size of an element is generally small if it is close to the surface. The general guideline is to let the current in each element be approximately the same according to its exponential decay. The maximum number of layers is limited to be 11 where the current in the innermost layer drops to 0.1 % of J_s. This means the centre of the conductor is hollowed if the current density decreases to 0.1 % before the depth reach to the conductor centre.

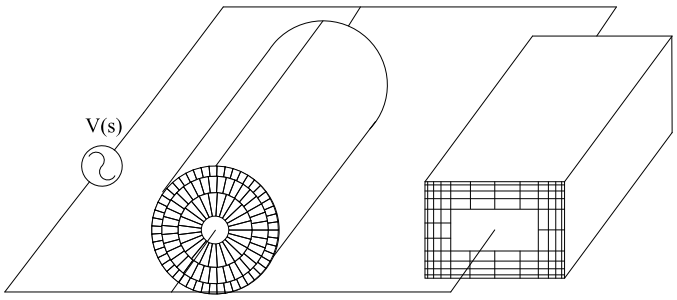

Figure 2. Meshing scheme for conductors with circular and rectangle cross sections.

After discretising wires, the current density in such small segments can be regarded as uniform. The resistance of each filament is given by

$$R = \frac{l}{\sigma \cdot S} \tag{4}$$

where σ is the conductivity of the wire and S is the area of the conductor cross section. Inductance of each segment can be determined using the Neumann integral formula. The point-matching method [20] is adopted to reduce a 4-fold integral to a 2-fold integral. Meanwhile, the average potential method is applied to ensure the accuracy of the integration.

For elements with the annular cross section, a formula for annular-filament inductance has been derived from the thin-wire formula of (7).

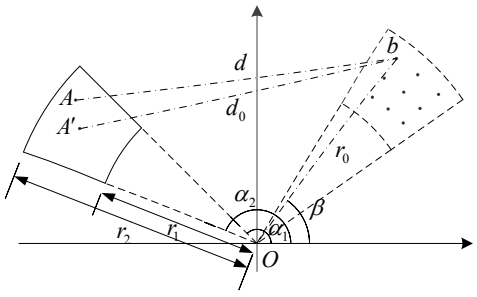

Figure 3. Geometric information of annular-multi filament cell.

Given by the geometry of the segments in Figure 3, inductance between annular segment A and filament b is expressed by

$$M_{sf} = \frac{\mu_0}{2\pi}\int_{\alpha_1}^{\alpha_2}\int_r \left[l \ln \frac{l+\sqrt{l^2+R^2}}{R} - \sqrt{l^2+R^2} + R \right] r dr d\theta \tag{5}$$

where, $R=\sqrt{r^2+r_0^2-2rr_0cos(\alpha-\beta)}$ is the distance between any point in field segment and source point. As $l \gg R$, (5) can be simplified as

$$M_{sf}=\frac{\mu_0}{2\pi}\int_{\alpha_1}^{\alpha_2}\int_r\left[l\ln\left(l+\sqrt{l^2+d_0^{\,2}}\right)-l\ln R-\sqrt{l^2+d_0^{\,2}}+d_0\right]rdrd\theta \tag{6}$$

where d_0 is the distance between the center of field segment and source point. Then (6) can be integrated analytically over r as

$$\begin{aligned}M_{sf}=&\frac{\mu_0}{4\pi}\int_{\alpha_1}^{\alpha}\left\{r^2\left[l\ln(l+\sqrt{l^2+d^2})-\sqrt{l^2+d^2}+d\right]+\frac{l}{2}\left(r^2+2rr_0\cos\theta\right)-l\left(r^2-r_0^2\cos 2\theta\right)\ln d\right.\\&\left.+2lr_0^2\sin\theta\cos\theta\arctan\frac{r-r_0\cos\theta}{r_0\sin\theta}\right\}d\theta\Bigg|_{r_1}^{r_2}\end{aligned} \tag{7}$$

where r_1 and r_2 are the inner and outer radius of the source segment, and r_0 is the radius to the center of the field element. Inductance is obtained by integrating over θ using numerical method. Both self and mutual inductance can be calculated by the above formula.

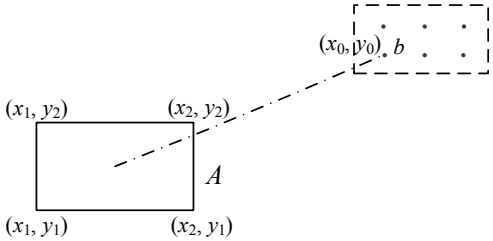

Figure 4. Geometric information of rectangle-multi filament cell.

For elements with the rectangular cross section, a rectangle-filament integral for inductance [21] is employed. As displayed in Figure 4, inductance between segment A and filament b is given in the form of

$$M_{sf}=\sum_{i=1}^{2}\sum_{j=1}^{2}(-1)^{i+j}\,g(q_i,r_j) \tag{8}$$

where $q_i=x_i-x_0$, $r_i=y_i-y_0$, and

$$\begin{aligned}g(q,r)=&\left(l^2-\frac{r^2}{3}\right)q\cdot\ln\left(r+D\right)+\left(l^2-\frac{r^2}{3}\right)r\cdot\ln\left(q+D\right)+qrl\cdot\ln\frac{D+l}{D-l}-\frac{2qr}{3}D-\frac{l^3}{3}\tan^{-1}\frac{qr}{l\cdot D}\\&-q^2l\tan^{-1}\frac{yl}{q\cdot D}-r^2l\tan^{-1}\frac{ql}{r\cdot D}+\frac{q^2}{3}\ln\left(y+d\right)+\frac{r^2}{3}\ln\left(q+d\right)+\frac{2qrd}{3}\end{aligned}$$

$$D=\sqrt{q^2+r^2+l^2}\qquad\qquad d=\sqrt{q^2+r^2}$$

In both cases, the source object B is represented as a group of filaments. Then, by taking the average of all segment-filament formula, the following is obtained

$$L_{ij}=\frac{\sum_{i}^{N_f}\left(M_{sf}\right)_i}{N_f} \tag{9}$$

where L_{ij} is the mutual inductance between segments for $i\neq j$ and self-inductance for $i=j$, and N_f is the number of filaments in target object. M_{af} is obtained using segment-filament formulas given in (7) and (8). For general segments, $N_f = 3\times2$ or $N_f = 2\times3$ is best suitable for calculation in our meshing scheme. As matter of the fact, (9) is a simplified type of geometrical mean distance method [22].

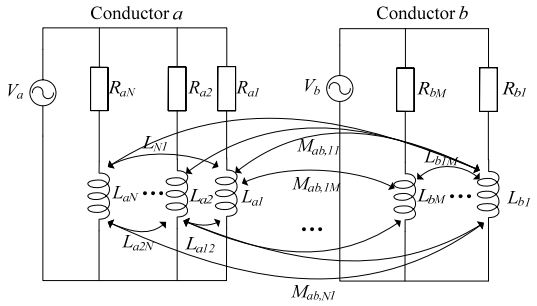

Figure 5. Equivalent circuit network for the segment of a two-conductor case.

After calculating all the partial elements, a circuit network can be then established as shown in Figure 5 for a two-conductor system. Wire *a* and *b* are discretized into *N* and *M* segments respectively. Each segment is represented by its DC resistance (R_{xx}) and partial inductance (L_{xx}) computed by (9). The mutual inductance (M_{xx}) between different segments is also calculated using (9). Write the voltage current relation for the two wires in the matrix form we have

$$\begin{bmatrix} \mathbf{R_a} + s\mathbf{L_a} & \mathbf{M_{ab}} \\ \mathbf{M_{ab}^T} & \mathbf{R_b} + s\mathbf{L_b} \end{bmatrix} \begin{bmatrix} \mathbf{I_a} \\ \mathbf{I_b} \end{bmatrix} = \begin{bmatrix} V_1 \cdot \mathbf{1_N} \\ V_2 \cdot \mathbf{1_M} \end{bmatrix} \tag{10}$$

where $\mathbf{R_x}$ is the diagonal matrix with DC resistance, $\mathbf{L_x}$ is the inductance matrix composed by the self and mutual inductance of the segment within a same conductor, $\mathbf{M_{xy}}$ represents the coupling between segments belonging to different conductors, $\mathbf{I_x}$ is the vector representing the current in each segment branch, $\mathbf{1_N}$ and $\mathbf{1_M}$ are vector of all ones with the dimensions of *N* x 1 and *M* x 1, V_x is the voltage source added to the conductor, and superscript *a* and *b* indicates the index of two conductors.

Taking advantages of the fact that all segments are equivalent to the branches connected in parallel [x], the currents in the segments can be calculated by the inverse of (10) as

$$\begin{bmatrix} \mathbf{I_a} \\ \mathbf{I_b} \end{bmatrix} = \begin{bmatrix} \mathbf{R_a} + s\mathbf{L_a} & \mathbf{M_{ab}} \\ \mathbf{M_{ab}^T} & \mathbf{R_b} + s\mathbf{L_b} \end{bmatrix}^{-1} \begin{bmatrix} V_1 \cdot \mathbf{1_N} \\ V_2 \cdot \mathbf{1_M} \end{bmatrix} \tag{11}$$

The total current (I_{xT}) in each wire can be computed by summing the currents in all segments of one wire, which can be written in matrix form as

$$\begin{bmatrix} I_{aT} \\ I_{bT} \end{bmatrix} = \begin{bmatrix} \mathbf{1_N} & \mathbf{0_N} \\ \mathbf{0_M} & \mathbf{1_M} \end{bmatrix}^T \begin{bmatrix} \mathbf{R_a} + s\mathbf{L_a} & \mathbf{M_{ab}} \\ \mathbf{M_{ab}^T} & \mathbf{R_b} + s\mathbf{L_b} \end{bmatrix}^{-1} \begin{bmatrix} \mathbf{1_N} & \mathbf{0_N} \\ \mathbf{0_M} & \mathbf{1_M} \end{bmatrix} \begin{bmatrix} V_1 \\ V_2 \end{bmatrix} \tag{12}$$

Therefore, the total impedance of the two-wire system is obtained as

$$\mathbf{Z_{abT}} = \begin{bmatrix} \mathbf{1_N} & \mathbf{0_N} \\ \mathbf{0_M} & \mathbf{1_M} \end{bmatrix}^T \begin{bmatrix} \mathbf{R_a} + s\mathbf{L_a} & \mathbf{M_{ab}} \\ \mathbf{M_{ab}^T} & \mathbf{R_b} + s\mathbf{L_b} \end{bmatrix}^{-1} \begin{bmatrix} \mathbf{1_N} & \mathbf{0_N} \\ \mathbf{0_M} & \mathbf{1_M} \end{bmatrix} \tag{13}$$

The above procedure for the calculation of two conductor case can be extended to the more general situations. The total impedance matrix $\mathbf{Z_T}$ of a system with multiple conductors can be calculated using the discretization method by

$$\mathbf{Z_T} = \left[\mathbf{B} \cdot \left(\mathbf{R_S} + s\mathbf{L_S} \right)^{-1} \cdot \mathbf{B}^{\mathbf{T}} \right]^{-1} \tag{14}$$

where $\mathbf{Z_T}$ is the total impedance matrix of the conductors with dimensions of $N_C \times N_C$, $\mathbf{R_S}$ is the diagonal resistance matrix of the discretized segments $N_S \times N_S$, $\mathbf{L_S}$ is the inductance matrix of the segments which including the mutual coupling terms between segments belonging to different conductors, and $\mathbf{B}$ is the selection matrix with $N_S \times N_C$ in which the elements in *k*th row *j*th column is 1 if the *j*th segment belongs to the *k*th conductor as $\mathbf{B}=[\mathbf{1_N}\ \mathbf{0_N};\ \mathbf{0_M}\ \mathbf{1_M}]$ in (13) for the two-conductor system. N_C indicates the number of the conductors and N_S represents the number of the segments after discretization.

2.3 Equivalent Circuit Model

The frequency dependent impedance matrix can be described by an equivalent network which is solved in time domain. Vector Fitting Algorithm (VF) [23] is adopted to generate the rational approximation of the impedance matrix.

The impedance matrix is calculated at several frequencies and approximated with rational functions in the form of pole residue terms as

$$Z(s) = R_0 + sL_0 + \sum_{m=1}^{N} \frac{s}{s - p_m} R_m \tag{15}$$

where the terms R_0 and L_0 are constant, and R_m and p_m are the mth residue and pole which have been extracted by VF. Expression (15) can be transformed into SPICE compatible form as [24, 25]

$$Z(s) = \bar{R}_0 + sL_0 + \sum_{m=1}^{N} \frac{s}{s - p_m} \bar{R}_m \tag{16}$$

where

$$\bar{R}_0 = R_0 - \sum_{m=1}^{N} \frac{1}{p_m} R_m \quad \bar{R}_m = \frac{1}{p_m} R_m \quad \bar{L}_m = -\frac{1}{p_m} \bar{R}_m$$

In contrast to the traditional VF expression, $\bar{R}_0$ and L_0 equals to DC resistance and the external inductance of the conductor. As normal conductors are well linearly parameterized, no complex poles exist. Thus, we employ a simplified form of the vector fitting equivalent circuit as shown Figure 6 in the calculation. According to our study, mutual inductance varies slightly with the frequency. Thus, the mutual couplings can simply be represented by a constant value as M_{ij}.

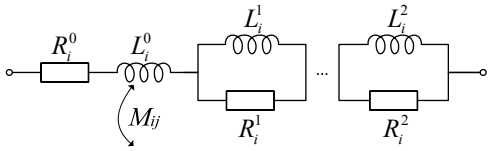

Figure 6. Circuit represetation of vector fitting approximation.

III. VERIFICATION

In this section, the proposed method is verified both numerically and experimentally. The proposed method is firstly compared with analytic formulas of skin effect. Isolated round wires and round tube are calculated by both two methods, where analytical results are adopted as the reference. Then, a laboratory experiment of closely spaced conductors is investigated by comparison of measurement and numerical methods.

3.1 Numerical Verification

To verify the proposed method and formulas, the proposed method is compared with analytical formulas for skin effect. Both isolated round wire and shell tube with information listed in Table II are investigated. Internal impedance of round wires is well developed as [13]

$$Z_{in} = \begin{cases} \dfrac{j\omega\mu}{2\pi R_a} \dfrac{I_0(a)}{I_1(a)} & \text{solid wire} \\ -\dfrac{j\omega\mu}{2\pi R_b} \dfrac{I_0(a)K_1(b) + K_0(a)I_1(b)}{K_1(a)I_1(b) - I_1(a)K_1(b)} & \text{shell tube} \end{cases} \quad \text{for} \tag{17}$$

where $K_n(\cdot)$ and $I_n(\cdot)$ are modified Bessel functions of order n with argument $R_r = (1+j)\cdot r/\delta$ in which δ is shin depth, subscripts a and b refer to the outer and inner radius of the wire.

Resistance of a round wire is the real part of the internal impedance. The inductance is the summation of internal inductance (image part of the internal impedance) and external inductance, which is expressed as

$$L_{ext} = \frac{\mu l}{2\pi} \left[\ln\left(\frac{l}{a} + \sqrt{1 + \frac{l^2}{a^2}} \right) - \sqrt{1 + \frac{a^2}{l^2}} + \frac{a}{l} \right] \tag{18}$$

TABLE II. MATERIAL AND GEOMETRIC INFORMATION OF CONDUCTORS

Material	DC Resistivity (mΩ/m)	Conductivity (S/m)	Outer Radius (mm)	Inner Radius (mm)	Length (m)
Round wire	0.195	5.80E+07	5	0	5
Round tube	0.098	5.80E+07	15	13	5

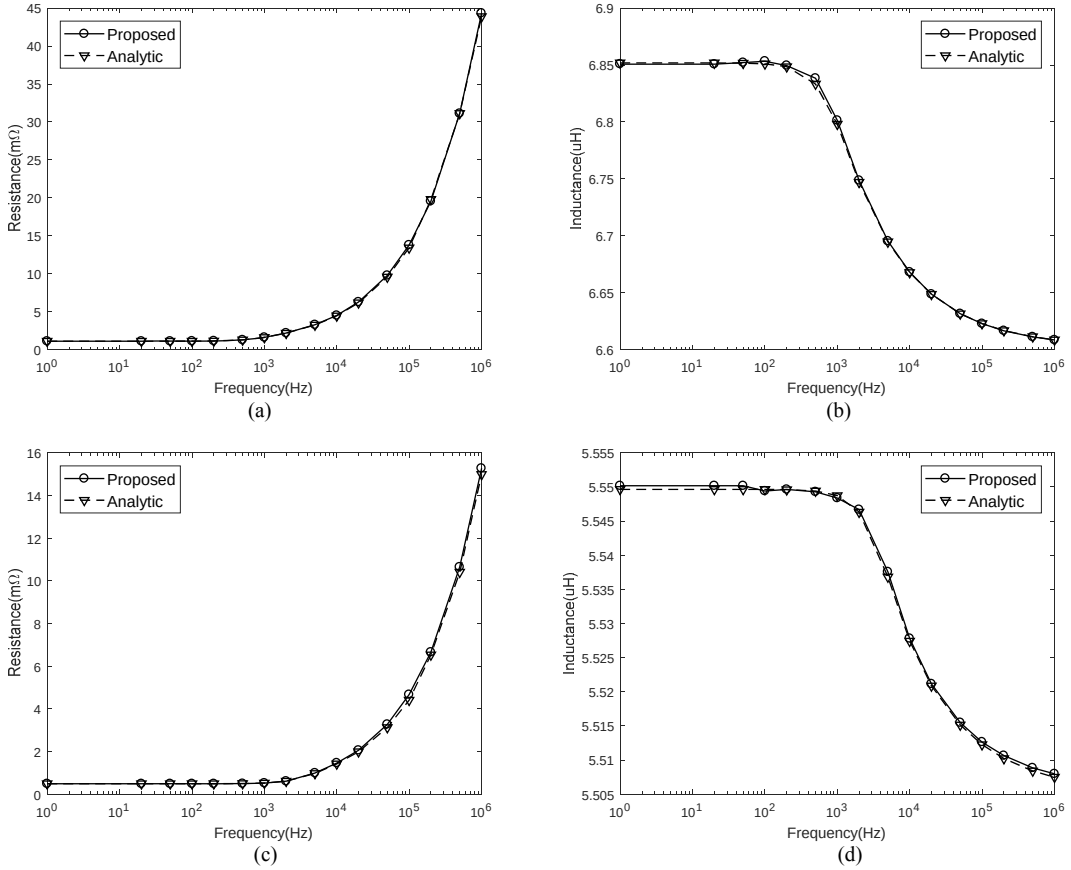

Figure 7. Reuslts comparison between proposed method and analytical formulas. (a) Resistance comparion for a round wire. (b) Inductance comparison for a round wire. (c) Resistance comparison for a round tube. (d) Inductance comparison for a round tube.

Calculated resistance and inductance curves are shown in Figure 7. Figure. 7(a) and 7(b) are the comparison results for round wire, while, comparison results for round tube are displayed in 7(c) and 7(d). Results obtained using proposed method match well with the analytic results in both cases.

3.2 Laboratory Experiment

An experiment was carried out in the laboratory to verify the proposed modelling procedure. This experimental arrangement was designed in such a way that proximity effect can be obviously observed. The system consisted of three aluminum tubes and a rectangular loop of thin conductors as shown in Figure 8. One side of the thin-wire loop were connected with three symmetrically placed tubes in parallel. The aluminum tubes were 3m in length and the thin conductor loop was 3 m (length) × 1 m (width). Table III shows the geometric and material information of the conductors used.

An 8/20 μs impulse current, which was generated from a pulse generator, was injected into the loop. In the experiment, the total current and the current in each branch were measured with Techtronic digital oscilloscope TDS3032C together with a current transducer Pearson 2877.

TABLE III. MATERIAL AND GEOMETRIC INFORMATION OF CONDUCTORS

Material	DC Resistivity (mΩ/m)	Conductivity (S/m)	Outer Radius (mm)	Inner Radius (mm)	Length (m)
Copper wire	6.898	5.80E+07	0.892	0	3
Al tube	0.468	3.78E+07	9.5	8.5	3

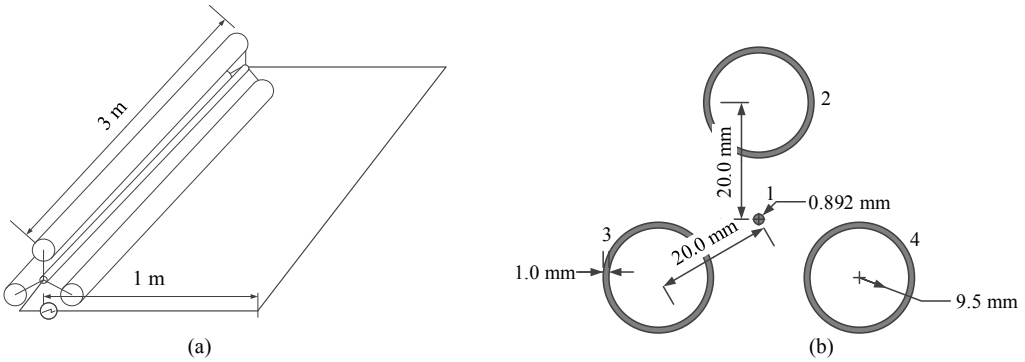

Figure 8. Configuration of the system under test. (a) System under test. (b) Cross section view.

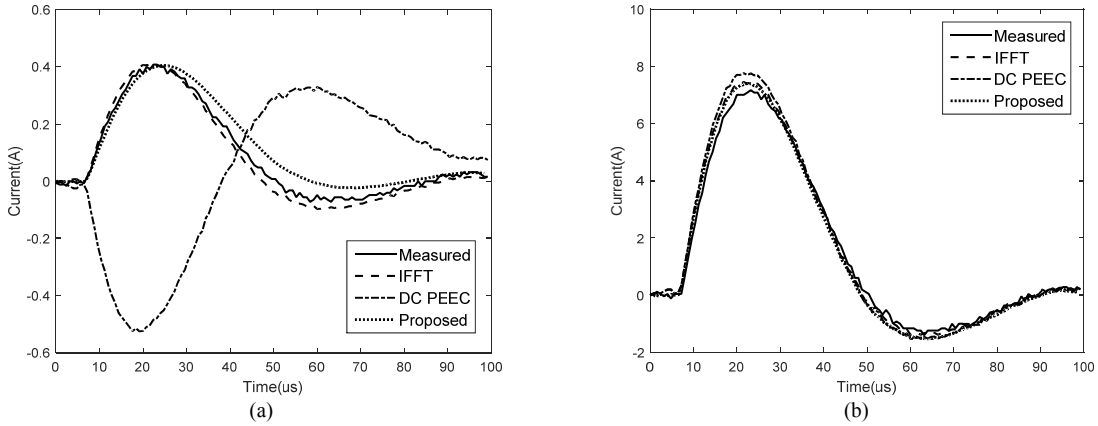

Figure 9. Surge currents in tested conductors by measurement and calculation. (a) Surge currents in cable 1 (wire). (b) Surge currents in cable 3 (tube).

Figure 9 shows both currents in the tube and thin wire measured in the experiment and calculated by the proposed procedure in time domain. For comparison, the results calculated in frequency domain and using equivalent approach was employed to compute the current in the tube as well as in the wire. In frequency domain solution, mutual inductance is frequency dependent and no simplification was applied. Meanwhile, the calculation using traditional PEEC elements, was also presented as "DC PEEC". In "DC PEEC", the resistance and inductance are obtained by the DC resistance and filament inductance formulas, respectively. Both skin and proximity effects are not considered in this method. The filament assumption is valid for far apart conductors [26], while, it will lead to a significant error for closely spaced conductors.

The total impulse current measured was 23.5A (peak). It is found in the figure that the waveforms obtained from the experiment and proposed PEEC model match very well. The differences of the peak current in the tube and the wire are less than 3% and 1%, respectively. The error of the wire current in the fall edge raised up a bit but the calculated result still matched well with the measured result. It is also noted that the proposed time-domain model performs as accuracy as the frequency-domain model. This indicates that the mutual inductance varied slightly with the frequency and can be replaced with a constant value. It is noted that there is a false negative peak in the wire current obtained by the DC PEEC method (Fig. 9(a)). This indicates that it is necessary to take into account the proximity effect in the calculation for closely spaced wires.

4 Analysis of Lightning Currents in Practical Cable Installations

In previous work, only cables are analyzed to represent a practical system which is obviously not sufficient. We conduct a series of transient current simulations with practical cable configurations. Three different configurations are analyzed and compared in this section:

1) Typical cable installation in a radio base station;
2) Cable installation with the communication tower;
3) Cables and tower with SPDs being installed.

The cross section view of the configuration (1) is displayed in Figure 10(c). Six coaxial cables (COX) and one shielded two-core power cable (SDC), are mounted on a cable ladder. The ladder has a nominal width of 300 mm and each cable ladder consists of two "L" shaped side rails with 50 mm in width and 5 mm in thickness. The detail information of the cables is listed in Table IV. All these cables and ladder rails are assumed to be 22.5 m long. The cables are normally terminated at both ends with electronic devices or protective devices. As the lightning strikes usually lead to a phase-to-ground fault, all cables are shorted together with the metal ladder at the two ends in the analysis.

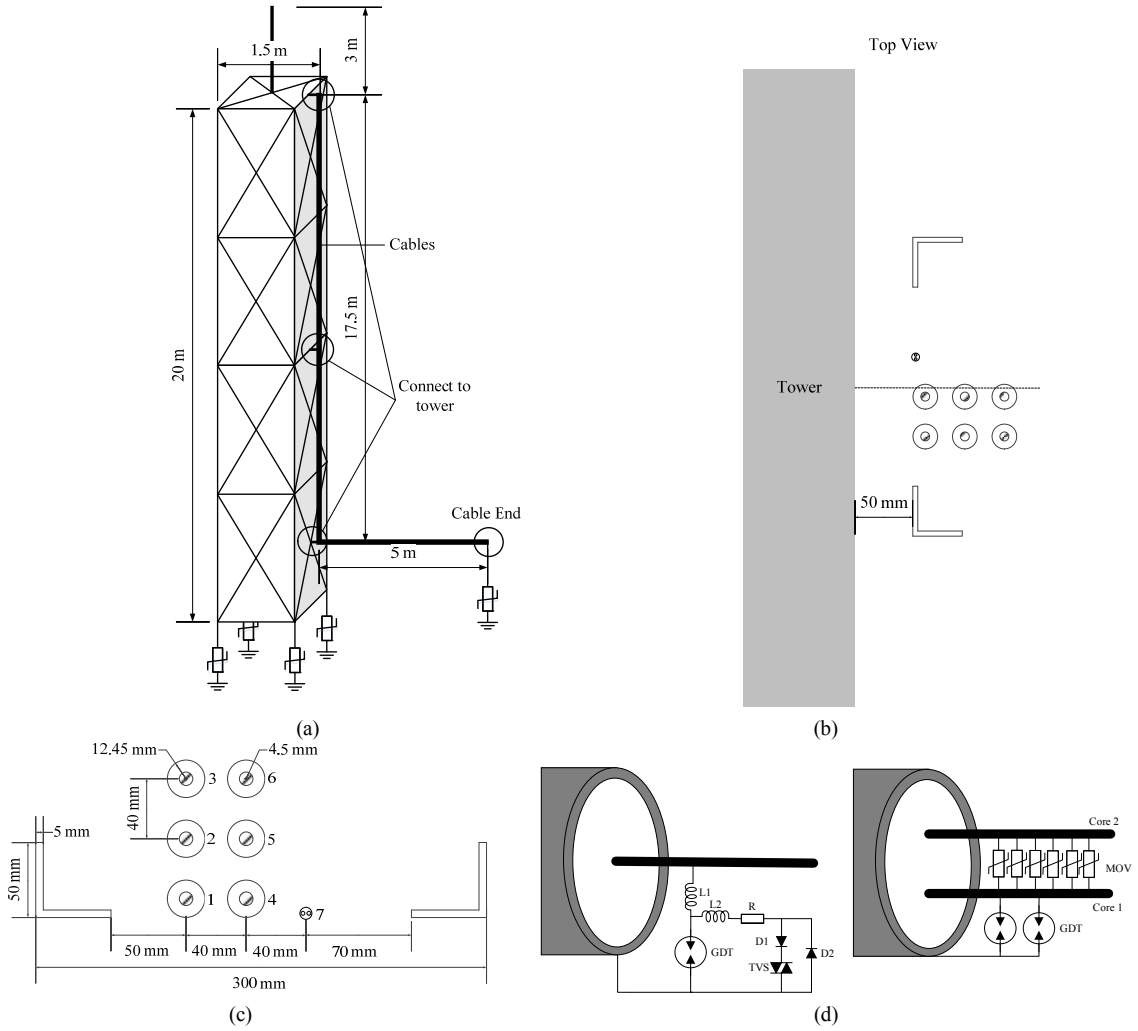

Figure 10. Configurations of a practical radio base system. (a) Configuration of the tower system. (b) Top view of the tower system. (b) Configuration of cables (cross section view). (c) Configuration of the protection block for coaxial and shield DC tower cables

In configuration (2), the cables in (1) are installed vertically along a 20 m communication tower. The tower is made of iron angles and a 3 m lightning rod as described in Table V. They are made of ferromagnetic materials, but behave like a linear magnetic material with constant relative permeability [27, 28] under lightning impulses. The cables are fixed on a cable rack 50 mm spaced from the tower. At the bottom of the tower, the cables are extended

horizontally for 5 m to the communication equipment which is not included in this study. Similar to configuration (1), all the cables are shorted together with the metal ladder at the two ends in the analysis. The cable ladder is connected to the tower at the top (20 m), middle (10 m) and the bottom (2.5 m). Both the tower legs and metal ladder are finally grounded through a resistance.

TABLE IV. MATERIAL AND GEOMETRIC INFORMATION OF CABLES

Material		Conductivity (*S/m*)	Outer Radius (*mm*)	Inner Radius (*mm*)
COX	Sheath	5.80E+07	12.45	11.65
	Core	5.80E+07	4.5	0
SDC	Sheath	3.78E+07	4	3.4
	Core	5.80E+07	1.3	0

TABLE V. MATERIAL INFORMATION OF TOWER AND THE ROD

Material	Relative Permeability	DC Resistivity (Ω/*m*)	Width/Outer Radius (*mm*)	Thick/Inner Radius (*mm*)
Tower	42	0.30	70	5
Rod	42	0.66	16	0

Configuration (3) includes a practical protection scheme for the system in radio base stations. All cables together with the metal ladder are shorted and connected to the tower on the top. SPDs are installed at the cable ends at the ground to protect the signal circuits connected. Different protection circuits are employed for coaxial cables and shielded DC cable as shown in Figure 9(d). In the coaxial cable, 90V GDT and 24A TVS are installed between its sheath and core through a RL circuit with R=0.25 Ω and $L1$= $L2$=2.2 μH. In the SDC cable, two 90V GDTs are connected between the sheath and core 1. Six S20K50 MOVs are connected in parallel between core 1 and core 2. The cable sheaths of all cables are connected to the ladder, finally to the ground.

In the simulation, the lightning return stroke current with the waveform of 8/20 μs and the magnitude of 20 kA is applied to the top of the lightning rod. The surge currents in both the cables and the tower are analyzed. As the cables and ladder are closely-spaced, the proposed discretization PEEC method is applied for modeling. The tower steel is represented with the skin effect model using the linear magnetic material [13, 27]. The skin effect model for a linear magnetic material has the same formulation as that for a non-magnetic material, except that the permeability μ_0 is replaced by $\mu_0\mu_r$. The mutual coupling between the power and cables was modeled using the Neumann formula. This is reasonable due to the tower conductors are oblique, perpendicular or far from the cables and the ladder that proximity effect among them is negligible. The system network is finally transformed into an equivalent circuit with frequency-independent circuit parameters using a vector fitting method. As the tower is a vertical structure, perfect ground is used in our computation [29]. Finally, the ground resistance is simplified as a nonlinear resistance recommended by CIGRE [30]

$$R_g(t) = \frac{R_i}{\sqrt{1 + i(t)/I_g}} \qquad I_g = \frac{E_0}{2\pi\sigma_g R_i^2} \tag{19}$$

where I_g is the current injected into the ground when the soil ionization happens, σ_g is the conductivity of the soil and E_0 is the critical electric field intensity of the soil. CIGRE recommends 400 kV/m for E_0. PSpice models for metal oxide varistors (MOV) [31, 32] and transient voltage suppress (TVS) [33] are used in Config.(c). After building up the model, the simulations are carried out in time domain using PSpice.

Figure 11 shows the peak values of the surge currents in these cables under 3 different configurations. The currents are normalized by the total current flowing through all cables. It is found that the current is distributed unevenly due to proximity effect. Cable 3 and 6, which are least influenced by proximity effect, carry larger currents than others. While, the cables located in the central area carry less current, such as Cable 2 and 5. The majority of the lightning current tends to be carried out by the cables in the outer layer. Comparison between the results obtained in Config.(1) and Config.(2) reveals that the tower increases the unbalance of the current distribution. More current moves to the outmost cables 3 and 6. In Config.(3), installed SPDs can suppress the surge current in cable cores which can protect the connected devices. However, as the currents are uneven distributed, the currents in the cores of cables 3 and 6 are significantly larger than that those in other cores. Engineers should pay more attention when dealing with the cables

in the outer layer. The current in SDC1, which represents RTN core line of a SDC, is not connected to electronic devices. Thus, SDC1 is not protected by SPDs, which results in larger current sharing.

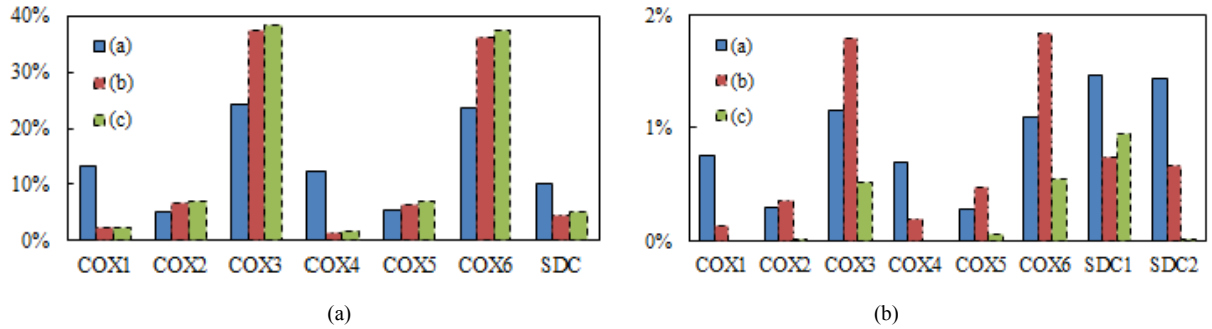

(a) (b)

Figure 11. Normalized peak current distribution in 3 configurations. (a) Distribution among cable sheaths. (b) Distribution among cable cores.(using black, white and grey figure)

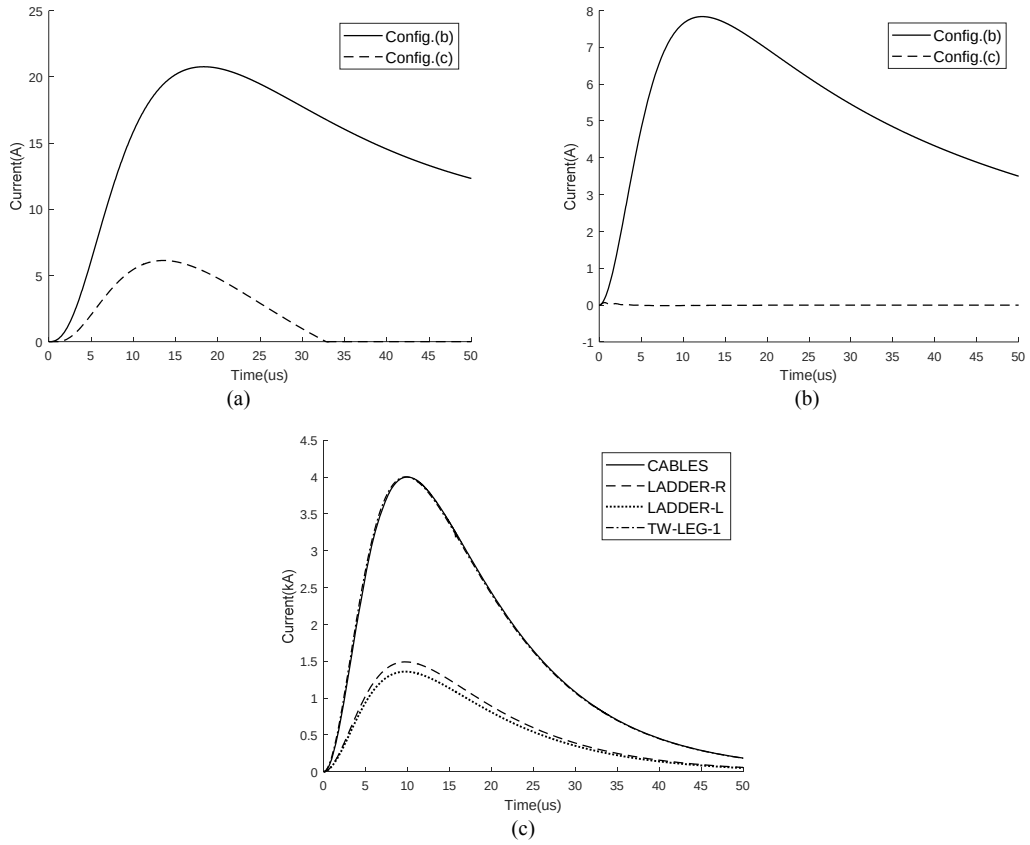

Figure 12. Current waveform in cables. (a) Currents in the core of Cable 3. (b) Currents in the core 2 of shielded DC cable. (c) Currents in cables, tower leg and cable ladders of Config.(c)

Figure 12(a) and Figure 12(b) show the waveforms of surge currents in core of cable 3 and core 2 of SDC cable. Under a 20 kA lightning strike, a transient current with the 5 A peak will flow into the connected equipment even SPDs are installed using the above protection scheme. It may cause damage to the system as more and more low voltage supply are employed. The current in the SDC core is suppressed from 8 A to nearly zero, and the protection is very effective. In Figure 12(c), currents flowing the tower and cable ladders are displayed. The tower legs, cable ladder and cables carry the currents with peak values of 4 kA, 3 kA and 1 kA, respectively.

5 CONCLUSIONS

In this paper conductors with strong skin and proximity effects wasa modeled using an equivalent circuit which was obtained by an extended PEEC method together with rational approximation. A skin-depth based discretization scheme was used to accelerate the computation. Comprehensive discussion on two aspects, skin effect vs proximity effect was presented. It is concluded that the skin effect model is sufficiently accurate for conductors with spacing of 2 × conductor diameters. For closely spaced conductors, the proximity effect must be considered to obtain accurate results. The proposed procedure was validated experimentally, and was applied to evaluate lightning current distribution among cables for radio base stations. According to the simulation results, currents distribute unevenly due to the proximity effect among cables. The presence of the tower further enhances the unbalance of the current distribution which should not be neglected in practical analysis. The cables in the outer location carry more currents than others. More attention should be paid to these cables, and a high degree of lightning transient protection would be necessary for these cables.

ACKNOWLEDGMENT

The work leading to this paper was supported by grants from the Research Grants Council of the HKSAR (Project No. 5148/13E and 152038/15E).

REFERENCES

[1] A. Tatematsu, K. Yamazaki, and H. Matsumoto, "Lightning surge analysis of a microwave relay station using the FDTD method," *IEEE Transactions on Electromagnetic Compatibility,* vol. 57, no. 6, pp. 1616-1626, Dec 2015.

[2] H. Chen, Z. Qin, Y. Du, Q. Wang, and Y. Ding, "TAES: A PEEC-based tool for transient simulation," in *2016 Asia-Pacific International Symposium on Electromagnetic Compatibility (APEMC)*, 2016, vol. 1, pp. 676-678: IEEE.

[3] U. S. Gudmundsdottir, "Proximity effect in fast transient simulations of an underground transmission cable," *Electric Power Systems Research,* vol. 115, pp. 50-56, 10// 2014.

[4] H. Chen, Y. Du, and M. Chen, "Lightning current among closely-spaced cables," in *2014 International Conference on Lightning Protection (ICLP)*, 2014, pp. 412-417.

[5] P. N. Mikropoulos, T. E. Tsovilis, and S. G. Koutoula, "Lightning performance of distribution transformer feeding GSM base station," *IEEE Transactions on Power Delivery,* vol. 29, no. 6, pp. 2570-2579, Dec 2014.

[6] C. R. Paul, *Analysis of multiconductor transmission lines*. John Wiley & Sons, 2008.

[7] J. P. A. Bastos and N. Sadowski, *Electromagnetic modeling by finite element methods*. CRC press, 2003.

[8] K. Ferkal, M. Poloujadoff, and E. Dorison, "Proximity effect and eddy current losses in insulated cables," (in English), *IEEE Transactions on Power Delivery,* vol. 11, no. 3, pp. 1171-1178, Jul 1996.

[9] T. Noda, A. Tatematsu, and S. Yokoyama, "Improvements of an FDTD-based surge simulation code and its application to the lightning overvoltage calculation of a transmission tower," (in English), *Electric Power Systems Research,* vol. 77, no. 11, pp. 1495-1500, Sep 2007.

[10] G. Antonini, S. Cristina, and A. Orlandi, "PEEC modeling of lightning protection systems and coupling to coaxial cables," *IEEE Transactions on Electromagnetic Compatibility,* vol. 40, no. 4, pp. 481-491, Nov 1998.

[11] M. E. Verbeek, "Partial element equivalent circuit (PEEC) models for on-chip passives and interconnects," *International Journal of Numerical Modelling: Electronic Networks, Devices and Fields,* vol. 17, no. 1, pp. 61-84, 2004.

[12] A. E. Ruehli, G. Antonini, and L. J. Jiang, "Skin-Effect Loss Models for Time- and Frequency-Domain PEEC Solver," *Proceedings of the IEEE,* vol. 101, no. 2, pp. 451-472, Feb 2013.

[13] S. A. Schelkunoff, "The Electromagnetic Theory of Coaxial Transmission Lines and Cylindrical Shields," *Bell System Technical Journal,* vol. 13, no. 4, pp. 532-579, 1934.

[14] H. A. Wheeler, "Formulas for the Skin Effect," *Proceedings of the IRE,* vol. 30, no. 9, pp. 412-424, 1942.

[15] A. E. Ruehli, "Inductance Calculations in a Complex Integrated-Circuit Environment," *IBM Journal of Research and Development,* vol. 16, no. 5, pp. 470-&, 1972.

[16] H. Heeb and A. E. Ruehli, "Three-dimensional interconnect analysis using partial element equivalent circuits," *IEEE Transactions on Circuits & Systems I Fundamental Theory & Applications,* vol. CAS-39, no. 11, pp. 974-982, 1992.

[17] B. Archambeault, C. Brench, and O. M. Ramahi, *EMI/EMC Computational Modeling Handbook*. Springer US, 2001, p. 19.

[18] W. C. Chew, M. S. Tong, and B. Hu, "Integral Equation Methods for Electromagnetic and Elastic Waves," *Synthesis Lectures on Computational Electromagnetics,* vol. 3, no. 1, pp. 1-241, 2008/01/01 2008.

[19] C. R. Paul, *Introduction to electromagnetic compatibility*. John Wiley & Sons, 2006.

[20] R. F. Harrington, *Time-harmonic electromagnetic fields*. Wiley-IEEE Press, 2001.

[21] C. Hoer and C. Love, "Exact Inductance Equations for Rectangular Conductors with Applications to More Complicated Geometries," (in English), *Journal of Research of the National Bureau of Standards Section C-Engineering and Instrumentation,* vol. C 69, no. 2, pp. 127-+, 1965.

[22] F. W. Grover, *Inductance calculations: working formulas and tables*. Dover, 1946.

[23] B. Gustavsen and A. Semlyen, "Rational approximation of frequency domain responses by vector fitting," *IEEE Transactions on Power Delivery,* vol. 14, no. 3, pp. 1052-1061, Jul 1999.

[24] K. M. Coperich, J. Morsey, V. I. Okhmatovski, A. C. Cangellaris, and D. E. Ruehli, "Systematic development of transmission-line models for interconnects with frequency-dependent losses," *IEEE Transactions on Microwave Theory and Techniques,* vol. 49, no. 10, pp. 1677-1685, Oct 2001.

[25] D. Su, B. Li, J. Wang, and X. Song, "Passivity enforced circuit model of frequency-domain responses with source elements," *International Journal of Numerical Modelling: Electronic Networks, Devices and Fields,* pp. n/a-n/a, 2016.

[26] Y. Du and M. L. Chen, "Influence of Building Structures on the Lightning Return Stroke Current," *IEEE Transactions on Power Delivery,* vol. 25, no. 1, pp. 307-315, 2010.
[27] H. Chen and Y. Du, "Model of Ferromagnetic Steels for Lightning Transient Analysis," *IET Science, Measurement & Technology,* 2017.
[28] H. Chen and Y.-P. Du, "Simulation of transients in electrical systems with ferromagnetic steels," presented at the 2016 Progress in Electromagnetic Research Symposium (PIERS), 2016.
[29] Y. Du, X. Wang, and M. Chen, "Transient surge impedance of a vertical conductor over the ground," *Electric Power Systems Research,* vol. 94, pp. 106-112, 1// 2013.
[30] L. Grcev, "Modeling of Grounding Electrodes Under Lightning Currents," *IEEE Transactions on Electromagnetic Compatibility,* vol. 51, no. 3, pp. 559-571, Aug 2009.
[31] A. EPCOS, "General technical information," *SIOV metal oxide varistors,* 2011.
[32] H. Chen and Y. Du, "A Comprehensive Study on the Nonlinear Behavior of Metal Oxide Varistors," *2016 33rd International Conference on Lightning Protection (ICLP),* 2016.
[33] J. Lepkowski and W. Lepkowski, "Evaluating TVS protection circuits with SPICE," *Power Electronics Technology,* vol. 32, no. 1, p. 44, 2006.
[34] Y. Du and J. Burnett, "Current distribution in single-core cables connected in parallel," *IEE Proc.-Gener.. Transm. Distrib.*, Vol. 148, No. 5, pp.406-412, Sept. 2001